Characterization of the Relationship of AAV Capsid Domain Swapping to Liver Transduction Efficiency

Xuan Shen[1,2], Terry Storm[1,2] and Mark A Kay[1,2]

[1]Department of Pediatrics, Stanford University, Stanford, California, USA; [2]Department of Genetics, Stanford University, Stanford, California, USA

Recombinant adeno-associated virus (AAV) vectors show promise for use in gene therapy. For liver-targeted gene transfer in animals, AAV vectors pseudotyped with the AAV serotype 8 (AAV8) capsid have definite advantages over the widely used but less efficient serotype AAV2, even though the capsid amino acid sequences are 82% conserved. To demonstrate the mechanism behind the higher liver transduction efficiency associated with AAV8 capsids, we adopted a domain-swapping strategy that would generate 27 chimeric capsid genes containing exchanged domains between AAV2 and AAV8. The resulting chimeric capsids were then used to package AAV genomes with a liver-specific human coagulation factor IX (hFIX) expression cassette. By comparing the transduction efficiencies between vectors pseudotyped with chimeric, AAV2 and AAV8 capsids, we found that the more efficient liver transduction achieved by AAV8 was closely related to the components of its interstrand Loop IV domain, particularly the subloops 1 and 4. These subloops are exposed on opposite sides of a threefold proximal peak on the virion surface, which may function as a critical structural determinant for AAV transduction. Because a single specific peptide component could not explain all the observed differences in the transduction parameters, we suggest that important subloop regions require interaction with other portions of the capsid for their functioning.

Received 11 April 2007; accepted 28 July 2007; advance online publication 28 August 2007. doi:10.1038/sj.mt.6300293

INTRODUCTION

Adeno-associated virus (AAV) is a non-pathogenic parvovirus that has become one of the most promising viral vectors for use in human gene therapy. Most of the early recombinant AAV vectors used in gene transfer studies were derived from AAV serotype 2 (AAV2). AAV2-based vectors are known to infect various types of both dividing and non-dividing mammalian cells, and have the potential for stable long-term transgene expression. However, AAV2 vectors are not always the optimal candidate for gene delivery applications, due to their restricted tissue tropism and low transduction efficiencies for certain targets. Naturally occurring antibodies against AAV2 capsids are estimated to exist in ~35–80% of the human population, thereby restricting the efficacy of AAV2 as a human gene therapy vector.[1–3] Currently, vectors based on other AAV serotypes are being studied for better gene transfer performance. In a scenario where repeated administrations are needed, AAV vectors of different serotypes would also be beneficial in order to escape the humoral immune response established due to prior AAV administrations.

In the past few years, a great number of new AAV serotypes have been isolated from various species.[4–10] AAV8, a serotype discovered in rhesus monkeys, has proved to be a remarkable alternative to AAV2 because it is able to mediate robust transgene expression in various tissues.[4,11,12] Particularly, for mouse liver transduction, only a small portion of the hepatocytes can be stably transduced with AAV2-based vectors, and transgene expression starts with a slow-rising lag phase after vector administration.[13] In contrast, the use of pseudotyped vectors of the AAV2 type genome, packaged in AAV8 capsids, is characterized by a more rapid rise in transgene expression as well as an unrestricted level of hepatocyte transduction, reaching levels that are ~20 times higher than found with prototype AAV2 vectors.[11] The capsid uncoating rate has been proposed to be the key factor differentiating their liver transduction efficiencies.[14] However, it is still unclear how the uncoating of AAV vectors takes place in cells and which cellular factors are involved.The question remains, as well, as to how exactly the uncoating rate is related to the structural differences in AAV capsids of different serotypes.

AAV viral particles are composed of a single-stranded DNA genome packaged in a non-enveloped icosahedral capsid. High-resolution structures of AAV2 and a few other serotypes have been determined by X-ray crystallography.[15–17] Preliminary X-ray crystallography data about the structure of AAV8 has also been reported,[18] although a detailed analysis and comparison with AAV2 is yet to be worked out. AAV capsid proteins can be divided into a series of secondary structures, including a group of conserved β strands and several highly diversified interstrand loop regions.[15] Conventionally these loops are grouped into five domains, or interstrand loop domains I–V,[19] as indicated in **Figure 1**. Since there is found to be more than

Correspondence: *Mark Kay, Department of Pediatrics and Department of Genetics, 300 Pasteur Drive, Room G305, Stanford University, Stanford, California 94305, USA. E-mail: markay@stanford.edu*

82% homology in the primary sequence between AAV2 and AAV8 capsid proteins, it can be assumed that the overall structure and domain composition of AAV8 capsids are similar to AAV2, whereas minor structural differences may exist in their serotype-specific sequences, especially in the interstrand loop domains. Domain swapping is a useful way of analyzing the structure–function relationship that exists among a group of homologous proteins. This method has been successfully used in the past to characterize the capsid determinants for the tissue tropism of AAV1.[20] In this study we adopted a similar strategy to determine the structural determinants of AAV8 capsids that might be responsible for high transduction efficiencies in the liver. A series of chimeric AAV capsid proteins was generated, by swapping domains between AAV2 and AAV8. By comparing the liver-targeted transductions mediated by vectors packaged in these chimeric capsids, we were able to identify the corresponding capsid regions that have a great influence on liver transduction efficiency.

RESULTS

Construction of chimeric AAV packaging helpers

To find out the structural basis for the differences between AAV2 and AAV8 in liver transduction, we generated a series of chimeric AAV *cap* genes by moving individual capsid domains from one serotype to the other. The alignment of the protein sequences of the two capsids is shown in **Figure 1**. To achieve such domain-swapping chimeras, we used a combination of polymerase chain reaction (PCR) and restriction digestion techniques to exchange fragments between AAV2 and AAV8 *cap* genes. The diagram in **Figure 2** shows the domain compositions of the 27 different chimeric *cap* gene constructs that were made for this study. These chimeric *cap* genes were all placed in the same AAV packaging helper backbone, which already carried an AAV2 *rep* gene for packaging recombinant AAV genomes with AAV2 inverted terminal repeats. These chimeric helpers were all confirmed by means of DNA sequencing, to be free of unexpected mutations, before they were tested for AAV genome packaging efficiencies.

```
                 ▶VP1
AAV-2:   1   MAADGYLPDWLEDTLSEGIRQWWKLKPGPPPPKPAERHKDDSRGLVLPGYKYLGPFNGLD  60
AAV-8:   1   MAADGYLPDWLEDNLSEGIREWWALKPGAPKPKANQQKQDDGRGLVLPGYKYLGPFNGLD  60

AAV-2:  61   KGEPVNEADAAALEHDKAYDRQLDSGDNPYLKYNHADAEFQERLKEDTSFGGNLGRAVFQ  120
AAV-8:  61   KGEPVNAADAAALEHDKAYDQQLQAGDNPYLRYNHADAEFQERLQEDTSFGGNLGRAVFQ  120
                           ▶VP2
AAV-2: 121  AKKRVLEPLGLVEEPVKTAPGKKRPVEHSPVE-PDSSSGTGKAGQQPARKRLNFGQTGDA  179
AAV-8: 121  AKKRVLEPLGLVEEGAKTAPGKKRPVEPSPQRSPDSSTGIGKKGQQPARKRLNFGQTGDS  180
                                 ▶VP3
AAV-2: 180  DSVPDPQPLGQPPAAPSGLGTNTMATGSGAPMADNNEGADGVGNSSGNWHCDSTWMGDRV  239
AAV-8: 181  ESVPDPQPLGEPPAAPSGVGPNTMAAGGGAPMADNNEGADGVGSSSGNWHCDSTWLGDRV  240
                  Loop I
AAV-2: 240  ITTSTRTWALPTYNNHLYKQISS--QSGASNDNHYFGYSTPWGYFDFNRFHCHFSPRDWQ  297
AAV-8: 241  ITTSTRTWALPTYNNHLYKQISNGTSGGATNDNTYFGYSTPWGYFDFNRFHCHFSPRDWQ  300
                                 Loop II                    Loop III
AAV-2: 298  RLINNNWGFRPKRLNFKLFNIQVKEVTQNDGTTTIANNLTSTVQVFTDSEYQLPYVLGSA  357
AAV-8: 301  RLINNNWGFRPKRLSFKLFNIQVKEVTQNEGTKTIANNLTSTIQVFTDSEYQLPYVLGSA  360
                                                      BsiW I
AAV-2: 358  HQGCLPPFPADVFMVPQYGYLTLNNGSQAVGRSSFYCLEYFPSQMLRTGNNFTFSYTFED  417
AAV-8: 361  HQGCLPPFPADVFMIPQYGYLTLNNGSQAVGRSSFYCLEYFPSQMLRTGNNFQFTYTFED  420
                  Loop IV                          Subloop 1
AAV-2: 418  VPFHSSYAHSQSLDRLMNPLIDQYLYYLSRTNTPSGTTTQSRLQFSQAGASDIRDQSRNW  477
AAV-8: 421  VPFHSSYAHSQSLDRLMNPLIDQYLYYLSRTQTTGGTANTQTLGFSQGGPNTMANQAKNW  480
                                 Subloop 2
AAV-2: 478  LPGPCYRQQRVSKTSADNNNSEYSWTGATKYHLNGRDSLVNPGPAMASHKDDEEKFFPQS  537
AAV-8: 481  LPGPCYRQQRVSTTTGQNNNSNFAWTAGTKYHLNGRNSLANPGIAMATHKDDEERFFPSN  540
                  Subloop 3
AAV-2: 538  GVLIFGKQGSEKTNVDIEKVMITDEEEIRTTNPVATEQYGSVSTNLQRGNRQAATADVNT  597
AAV-8: 541  GILIFGKQNAARDNADYSDVMLTSEEEIKTTNPVATEEYGIVADNLQQQNTAPQIGTVNS  600
                  Subloop 4                                      Loop V
AAV-2: 598  QGVLPGMVWQDRDVYLQGPIWAKIPHTDGHFHPSPLMGGFGLKHPPPQILIKNTPVPANP  657
AAV-8: 601  QGALPGMVWQNRDVYLQGPIWAKIPHTDGNFHPSPLMGGFGLKHPPPQILIKNTPVPADP  660

AAV-2: 658  STTFSAAKFASFITQYSTGQVSVEIEWELQKENSKRWNPEIQYTSNYNKSVNVDFTVDTN  717
AAV-8: 661  PTTFNQSKLNSFITQYSTGQVSVEIEWELQKENSKRWNPEIQYTSNYYKSTSVDFAVNTE  720

AAV-2: 718  GVYSEPRPIGTRYLTRNL  735
AAV-8: 721  GVYSEPRPIGTRYLTRNL  738

Identities = 611/738 (82%), Positives = 661/738 (88%), Gaps = 3/738 (0%)
```

Figure 1 Alignment of the primary protein sequences of adeno-associated virus serotype 2 (AAV2) and AAV8 capsids. Non-identical amino acid residues are highlighted in boldface. The N-termini for VP1, 2, and 3 are indicated by arrows pointing right. The five putative interstrand loop domains are enclosed in rectangular frames. Vertical dashed lines within the Loop IV domain divide its four subloops.

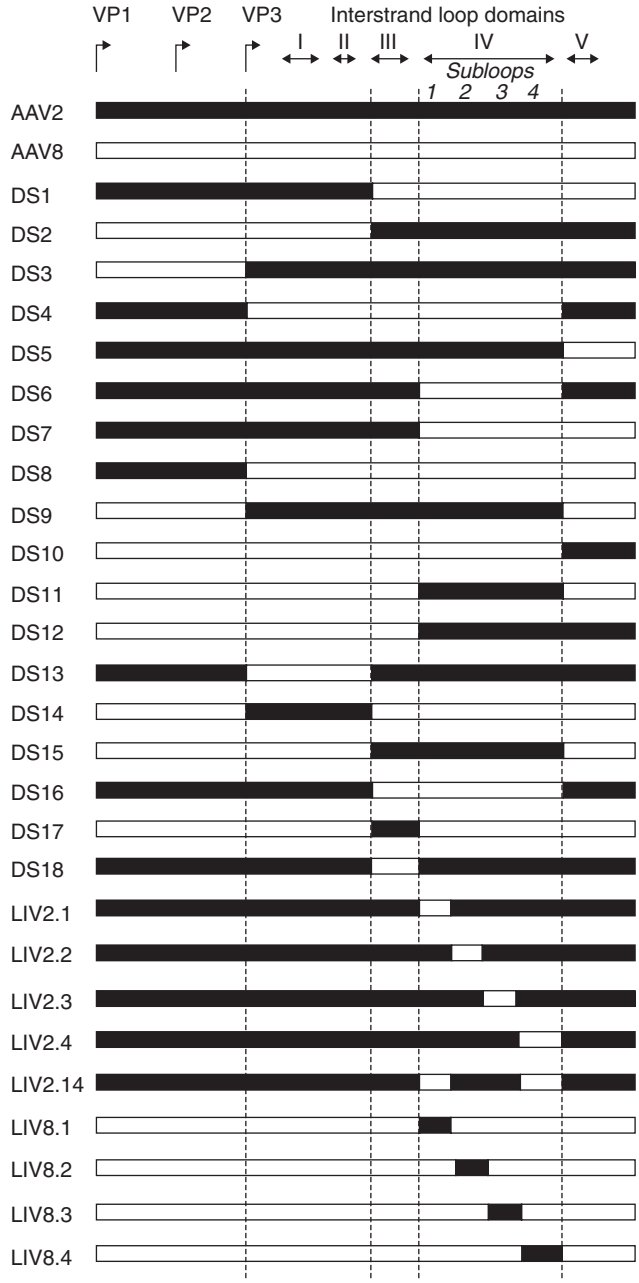

Figure 2 Diagram of the chimeric capsid constructs from domain swapping. Filled bars represent sequences from adeno-associated virus 2 (AAV2), whereas open bars represent sequences from AAV8. The N-termini for VP1, 2, and 3, five interstrand loop domains, and subloops in Loop IV domain are indicated at the top.

Evaluation of AAV production efficiencies of these chimeric capsid constructs

Because changes in the *cap* gene sequence could affect capsid protein expression, capsid assembly and eventually AAV genome packaging abilities, we checked the AAV production efficiencies of these chimeric AAV capsid constructs with a small-scale transfection assay. Triple-transfections of 293 cells were carried out in 6-cm culturing dishes with a chimeric AAV packaging helper and the two other plasmid components required for AAV production. The expression of VP1, 2, and 3 proteins of the AAV capsid, was tested by Western blot analysis and the genome packaging efficiencies were analyzed by dot-blot quantitation of capsid-protected AAV genomes in the post-transfection cell lysate. All the chimeric capsid constructs led to an expected expression of the three capsid proteins, with VP3 being the dominant form (data not shown); on the other hand, the yields of packaged AAV genomes, indicated by the viral genome-containing particle numbers on each 6-cm dish, varied significantly (**Figure 3**). In our control experiments, the wild-type AAV8 *cap* gene consistently produced approximately fourfold more viral particles than did the AAV2 *cap* gene, suggesting that certain sequence elements in the AAV-8 *cap* gene may contribute to better genome packaging abilities. The highest packaging efficiency achieved by these chimeric constructs was observed with DS17, which gave a viral genome titer similar to that of AAV8. This is not surprising because this specific chimeric capsid differs from the wild-type AAV8 only by three amino acid (a.a.) residues in the swapped region (a.a. 351–418). Most of the other domain-swapping chimeric constructs showed viral genome packaging efficiencies that varied in range between that of AAV2 and AAV8. However, a few chimeric capsid constructs produced even lower viral genome titers than that from AAV2. For example, the first two chimeric constructs, DS1 and DS2, generated by cutting the *cap* genes in the middle and ligating the N- and C-terminal fragments from different serotypes, produced ~50% lower viral titers than did AAV2. The lowest viral genome titer was observed with LIV2.2, generated by substituting the subloop 2 of Loop IV domain in AAV2 *cap* gene with the corresponding part from AAV8. It is not clear why the AAV packaging capabilities of these chimeric capsids were partially defective, nor is it as straightforward as finding a possible correlation between the packaging efficiency and specific *cap* gene sequences.

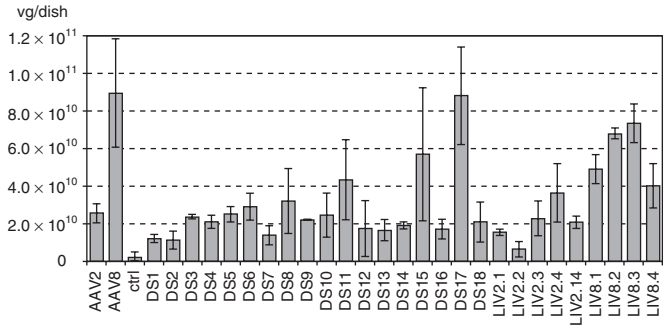

Figure 3 Comparison of adeno-associated virus (AAV) genome packaging efficiencies. The numbers of packaged AAV genomes per 6-cm dish from the chimeric capsid packaging helpers are compared with those from wild-type AAV2 and AAV8 capsid helpers. "ctrl(–)" means negative control where no packaging helper was added. The data shown are mean ± SD from at least three duplicate dishes. vg, vector genome.

In vivo mouse liver transduction by chimeric AAV vectors: importance of the interstrand Loop IV domain

For mouse liver transduction experiments, 1×10^{11} recombinant particles of each purified AAV vector was infused into the mouse liver vascular system through the portal vein. This administration route was favored (over the more convenient tail

vein intravenous injection method) in order to circumvent any possible transduction discrepancies introduced by the difference in vector infusion routes. It has been known that for mouse liver transduction, AAV2 vectors can be significantly less efficient when infused through peripheral routes such as the tail vein, than when infused directly into the liver vascular system by a portal vein injection.[21,22] However, this difference caused by the vector infusion route was not observed in the case of AAV8 vectors, for which transduction by means of either a portal vein or tail vein injection proved equally efficient.[11,23] Therefore, the portal vein injection route is likely to be a better choice to ensure a direct comparison of liver transduction efficiencies under optimal conditions for different chimeric vectors.

The transgene expression was monitored by measuring the human coagulation factor IX (hFIX) levels in the mouse plasma after administration of the portal vein injection. The hFIX expression profiles in mice infused with the chimeric vectors were analyzed and compared with those receiving the wild-type AAV2 and AAV8 vectors. AAV2-mediated transgene expression featured a slow onset or lag phase, meaning that after vector infusion the hFIX level took a few weeks to gradually increase before a stabilized level was obtained (~1,000 ng/ml). By contrast, AAV8-mediated expression rapidly reached a higher peak level in just a few days following vector infusion, and then remained at high levels with only a slight drop observed after a few weeks (**Figure 4**). The sustained hFIX levels of AAV8 vectors were ~10,000 ng/ml; this was at a tenfold higher level than that obtained with AAV2 vectors. The fast onset of transgene expression as well as the higher transduction efficiency have been described in the past,[11,24] and have been proposed to be related to the rapid uncoating rate of AAV8 vectors.[14]

The expression profiles of the chimeric AAV vectors are summarized in **Figure 4**. Four of the chimeric vectors demonstrated an AAV8-like robust liver transduction (DS8, DS10, DS14, and DS17 in **Figure 4a**). In these chimeric capsids, a.a. residues 1–210, 211–353, 354–421, and 645–738 of the AAV8 VP1 sequence were replaced by the corresponding AAV2 sequences respectively. Switching to AAV2 specific sequences in any of these regions did not affect the robust liver transduction observed with AAV8 vectors. These regions cover a large portion of the capsid sequence, including the N-terminal VP1/2 specific region, interstrand Loop I, II, III, and V domains. In contrast, if the Loop IV domain of AAV8 (a.a. 422–644) was replaced by the AAV2 sequence, the resulting chimeric vector became much less active in liver transduction (DS11 in **Figure 4a**). The corresponding plasma hFIX levels were even less than that obtained with AAV2, with a modest rise in the first 3 weeks followed by a slow decline before stabilizing at about the ~100 ng/ml level. Based on these results, the interstrand Loop IV domain seems to have a much greater influence on AAV transduction efficiencies than the other capsid regions.

On the other hand, a combined contribution from the other regions outside the Loop IV domain cannot be completely ruled out either. When the N-terminal half of the AAV8 capsid (a.a. 1–353) was replaced by AAV2 sequences, as in the chimeric construct DS1, the corresponding hFIX expression level became approximately five times lower than that of AAV8.

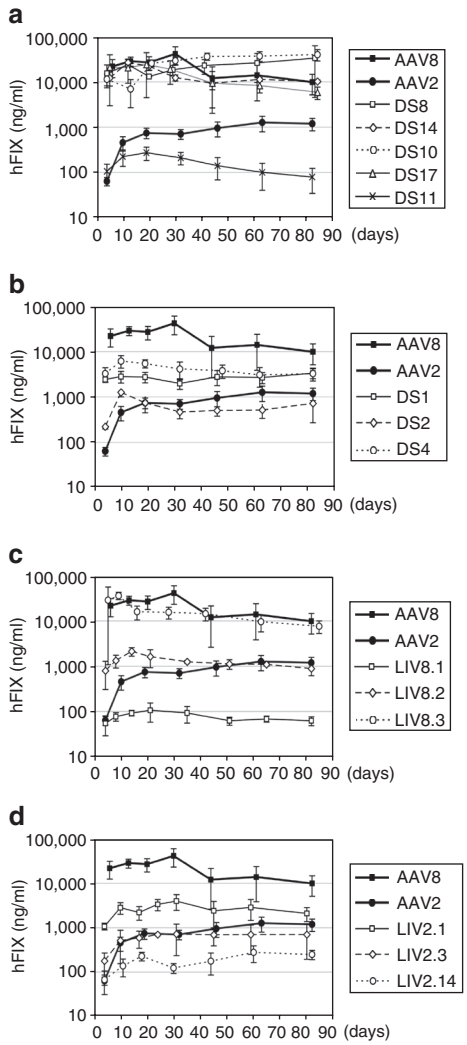

Figure 4 ***In vivo*** **human coagulation factor IX (hFIX) expression from chimeric adeno-associated virus (AAV) vectors.** C57BL/6 mice (n = 3) were injected through the portal vein with AAV vectors at a dose of 10^{11} vector genome per animal. Shown are the hFIX protein levels (mean ± SD) in mouse plasma (ng/ml) plotted versus time post vector injection (days). The data are divided into four subpanels, and hFIX expression from control vectors with wild-type AAV2 and AAV8 capsids is shown in each subpanel.

Similarly, some amount of drop in the transduction efficiency was observed with DS4, in which the N-terminal a.a. 1–210 and C-terminal a.a. 645–738 of AAV8 capsid were both replaced with corresponding AAV2 sequences (**Figure 4b**). However, for both DS1 and DS4, the hFIX expression profiles were still well above the level for AAV2, and featured an AAV8-like fast onset of transgene expression. In comparison, for the chimeric capsid DS2, which carries the N-terminal half (a.a. 1–353) from AAV8 and C-terminal half (a.a. 354–738) from AAV2, the hFIX expression was considerably less efficient and close to the level of AAV2. (**Figure 4b**) By comparing the transgene expression from DS1 and DS2, it can be concluded that the C-terminal half of the AAV capsid, where the Loop IV domain resides, was more important for determining liver transduction efficiencies.

Table 1 Biodistribution of AAV vector genomes[a]

	Liver	Pancreas	Spleen	Heart	Lung	Kidney	Intestine	Muscle
AAV2	0.4	<0.1[b]	<0.1	<0.1	nd[c]	<0.1	nd	<0.1
AAV8	6.6	nd	nd	<0.1	nd	nd	<0.1	nd
DS1	1.0	<0.1	<0.1	<0.1	nd	nd	<0.1	nd
DS2	0.5	nd	nd	nd	<0.1	nd	<0.1	nd
DS4	1.1	<0.1	<0.1	<0.1	nd	<0.1	<0.1	<0.1
DS6	nd	<0.1	nd	<0.1	nd	nd	nd	nd
DS8	2.3	nd	nd	<0.1	nd	nd	<0.1	nd
DS10	2.3	<0.1	nd	<0.1	<0.1	<0.1	<0.1	<0.1
DS11	<0.1	<0.1	<0.1	<0.1	<0.1	<0.1	nd	<0.1
DS14	1.5	<0.1	<0.1	<0.1	<0.1	<0.1	<0.1	<0.1
DS17	4.8	nd	nd	nd	<0.1	nd	nd	nd
LIV8.1	nd	nd	nd	nd	nd	nd	nd	nd
LIV8.2	0.4	nd	nd	nd	nd	nd	nd	nd
LIV8.3	2.7	nd	nd	nd	nd	nd	nd	nd
LIV8.4	nd	nd	nd	nd	nd	nd	nd	nd
LIV2.1	0.8	nd	nd	nd	nd	nd	nd	nd
LIV2.3	0.2	nd	nd	nd	nd	nd	nd	nd
LIV2.4	nd	nd	nd	nd	nd	nd	nd	nd
LIV2.14	0.1	0.1	nd	nd	<0.1	<0.1	<0.1	<0.1

[a]Adeno-associated virus (AAV) double-stranded vector genome (vg) numbers per diploid genome equivalent (ds-vg/dge) were quantitated by Southern blot for each tissue 3 months following portal vein infusion of 10^{11} vg AAV vectors. The shown values are averages from three animals. [b]Due to the sensitivity and accuracy limits of the assay, "<0.1" is assigned to detectable low values <0.1 ds-vg/dge. [c]"nd" means not detected. The sensitivity of the Southern blot assay is 0.03–0.1 ds-vg/dge.

Swapping interstrand Loop IV domain or its subloops could result in vector inactivation

An interesting phenomenon was noted when we examined the liver transduction efficiencies of chimeric vectors DS11 and DS6, in which the Loop IV domain of AAV8 or AAV2 was replaced with the corresponding part from the other serotype. The hFIX expression of chimeric vector DS11 was less robust than that of AAV2 (**Figure 4a**), suggesting that the swap of the AAV2 Loop IV domain with that of AAV8 may cause vector inactivation. This inactivation phenomenon was more obvious when we tested the transduction efficiency of DS6, in which the Loop IV domain of AAV2 capsid was replaced by its corresponding AAV8 sequence. Instead of showing AAV8-like robust transduction efficiency, this chimeric vector was highly inactive, with hFIX expression levels found constantly at well below 100 ng/ml (data not shown). The nature of such a low transduction activity is still indeterminate . Presumably, it was related to the complex structure of the Loop IV domain and its extensive interactions with other capsid regions.

In an attempt to better understand the influence on transduction efficiencies, of smaller structural elements in the large Loop IV domain, we examined hFIX transgene expression mediated by the subloop-swapping chimeric vectors (**Figure 4c** and **d**). As shown in **Figure 2**, LIV8.1–LIV8.4 were based on the AAV8 capsid with individual subloops in the Loop IV domain replaced with the AAV2 sequence, while LIV2.1–LIV2.4 and LIV2.14 were similar subloop-swapped chimeras based on the AAV2 capsid. Among the four subloops, subloop 3 did not seem to have a significant influence on the liver transduction efficiency. Swapping this subloop in either the AAV2 or AAV8 capsid did not result in a significant distinction from the corresponding wild-type capsid (LIV8.3 in **Figure 4c** and LIV2.3 in **Figure 4d**). Although the substitution of subloop 2 in the AAV8 capsid resulted in an almost 10-times drop in hFIX levels compared to AAV8 vectors, the fast onset of transgene expression was not affected (LIV8.2 in **Figure 4c**). The plasma hFIX level started and remained constant at ~1,000 ng/ml. Testing of LIV2.2 was hindered by its poor packaging efficiency and correspondingly low vector titer (**Figure 3**). However, in a separate experiment with a three times lower vector dose [3×10^{10} vector genome (vg) per mouse], our preliminary data indicated the transduction efficiency of LIV2.2 was comparable to that of AAV2 vectors (data not shown).

In comparison, substitution of subloop 1 or 4 resulted in more substantial changes in the transduction efficiency. LIV8.1 led to a highly diminished hFIX expression level of ~100 ng/ml (**Figure 4c**), indicating a loss of AAV8-like robust transduction activity and possible vector inactivation. On the other hand, LIV2.1 was able to transduce mouse liver several times more efficiently than could AAV2 (**Figure 4d**). These results suggest that subloop 1 probably plays a critical role in the determination of serotype-specific transduction performance. Subloop 4 substitution in both AAV2 and AAV8 (LIV2.4 and LIV8.4) resulted in vector inactivation with barely detectable hFIX expression levels (data not shown). Such inactivation suggests a different kind of role played by subloop 4, which probably

involves interactions with other capsid regions, but is also critical for the transduction performance. The concurrent substitution of both subloops 1 and 4 in the chimeric vector LIV2.14 did not fully relieve the inactivation effect, resulting in transgene expression still weaker than that of the AAV2 vectors (**Figure 4d**).

Differences in the transgene expression level by chimeric AAV vectors do not result from altered tissue tropism

Because the AAV genomes used in this study carried a liver-specific transgene expression cassette, only liver-targeted transduction could be evaluated in our experiments. It remained possible that the observed differences in transduction efficiencies were partially due to the changes in the liver uptake and tissue distribution pattern of these chimeric vectors. We performed Southern blot analysis on the genomic DNA extracted from various tissues and compared the differences in vector tropism (**Table 1**). For most of the chimeric vectors, the vg copy numbers in liver qualitatively correlated with the corresponding sustained hFIX expression levels. Although AAV genomes were detectable in some non-liver targets, the quantities were usually no more than 0.1 double-stranded vgs per diploid genome equivalent. This suggested that even though the tissue distribution patterns could be affected by domain swapping, the detectable changes in tissue tropism at this vector administration dose were minimal at best. More importantly, for those highly inefficient vectors such as DS6, LIV2.4, and LIV8.4, the extremely low vg copy numbers in the liver were not accompanied by correspondingly higher numbers of vg in other non-liver targets. Therefore, the low liver transduction efficiencies could not be explained by non-liver targeting.

DISCUSSION

Our study was aimed to discover the structural basis responsible for the contrasting differences in liver transduction between AAV2- and AAV8-based vectors. By studying a series of chimeric AAV capsids generated by swapping domains between AAV2 and AAV8, we were able to evaluate the importance of individual capsid domains in liver transduction; we identified the interstrand Loop IV domain as the most critical capsid region for determination of liver transduction efficiencies. Further analysis of the subloop-swapping chimeras revealed some of the specific roles that each subloop in the Loop IV domain plays in this process. In comparison to the minimal or moderate influence from subloops 2 and 3, subloops 1 and 4 played more critical roles in mouse liver transduction. Particularly, certain AAV8-specific sequence elements in subloop 1 seemed to be necessary but not sufficient to achieve the high liver transduction efficiencies observed with AAV8 vectors. The importance of the Loop IV domain in muscle transduction has been addressed in a previous study, using a similar domain swapping strategy between AAV1 and AAV2; the results of this study seemed to suggest that the Loop III and IV domains may be the major region responsible for the muscular tissue tropism of AAV1.[20] Taken together, it is plausible to speculate that the Loop IV domain may indeed be a key domain for all AAV serotypes. The highly diversified sequence of this domain may be the basis to determine AAV tissue tropism and other serotype-specific properties.

Despite its success in identifying the capsid regions responsible for efficient liver transduction, our approach still had some drawbacks. It is possible that the domain-swapping strategy may have oversimplified the complex structure of assembled AAV capsids. In an assembled capsid, amino acid residues located remotely in the primary sequences or from different subunits may come into spatial proximity to form a functional unit. To really understand the differences between AAV2 and AAV8 capsids, the complex three-dimensional structures and the extensive interactions in an assembled capsid would all need to be compared. In this study, molecular cloning without any functional selection pressure, were used to generate the domain-swapping chimeras. As a result, deficiencies in the capsid functions may have been introduced unintentionally. Indeed, we found that swapping the whole Loop IV domain or some of its subloops could cause unexpected inactivation of resulting chimeras, which made it more difficult to interpret the transduction data and establish connections between the structure and biological functions. Because we have not characterized all the critical steps in the transduction pathway, the transgene expression data is not enough for us to speculate on the biological basis for such inactivation effects. Presumably, because of the low sequence homology in the Loop IV domain, and the complexity of interactions involving its components, swapping sequences between AAV2 and AAV8 in this domain could cause unintended alteration of biologically critical structures that are dependent on other regions of the capsid. In summary, we believe that further study is required, whereby swapping from other capsid regions, in addition to those in subloops 1 and 4 in the Loop IV domain, should be compared in the same chimeric vector.

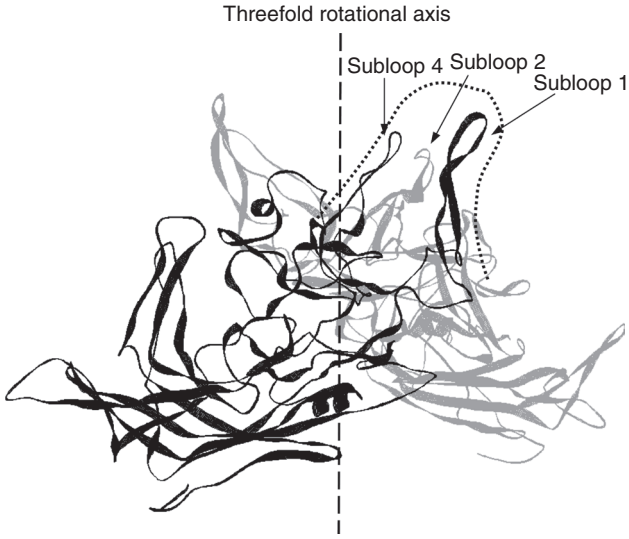

Figure 5 Three-dimensional illustration of subunit interactions at a threefold-proximal peak. Two neighboring capsid subunits, shown in black and gray ribbon forms respectively, interact with each other around a threefold rotational axis. The dotted line outlines the threefold-proximal peak, in which subloop 2 from one subunit is sandwiched between subloops 1 and 4 from the other subunit. The image was prepared with Swiss-Pdb Viewer[34] based on the coordinates of AAV2 structure (Protein data bank Accession No. 1LP3).

Of all the distinctive topological structures on the surface of assembled AAV capsids, we hypothesize that the threefold-proximal peaks may play a central role in the determination of transduction efficiencies. Protruding from the virion surface near the threefold rotational axes, these peaks are highly accessible to interacting host factors during AAV infection.[15] Based on the homology structural modeling analysis between AAV2 and AAV8, the overall topology of these threefold-proximal peaks and their components ought to be conserved between these two AAV serotypes. According to the known structure of AAV2, a threefold-proximal peak contains the following components from two neighboring capsid subunits. Subloops 1 and 4 of the Loop IV domain from the first subunit are located on the two opposite sides of the peak, whereas subloop 2 from the second subunit resides in between, to form the core of the peak. These three subloops constitute a sandwich-like structure (**Figure 5**). Our results point to the importance of subloops 1 and 4 in AAV transduction. The exposure of these two subloops on the surface of the threefold-proximal peaks is consistent with the central role of these peaks in AAV transduction. One can presume that interactions between the two exposed subloops and host cellular factors are critical for the AAV transduction process. Although direct interactions involving subloop 2 and host factors are probably limited due to its sandwiched position, this subloop may interact with its two exposed partners, thereby affecting their conformations and thus causing changes in AAV transduction. This hypothesis is in accordance with our *in vivo* chimera transduction results.

It remains to be investigated as to how these peak structures actually participate in the AAV infection process, and what host factors are involved. In the past, AAV capsid characterization studies have mostly focused on receptor binding and antigenic properties. For example, it is known that a heparin-binding motif exists in the AAV2 capsid, which involves several basic a.a. residues in the Loop IV domain that also includes two critical arginine residues in subloop 4.[25,26] Binding to a laminin receptor by AAV2 and AAV8 also involves the subloops in the Loop IV domain.[27] Therefore, sequence swapping in these subloop regions would probably change the receptor-binding properties of AAV vectors. However, other steps in the AAV infection pathway, such as endocytosis, intracellular trafficking, nuclear entry, and/or vector uncoating, have not been studied in detail. Of all the possible contributing mechanisms, we are most interested in the vector uncoating process, because the fast uncoating rate has been suggested to be the key to efficient AAV transduction in liver.[14] In this study we have not directly checked the nuclear uncoating rates of these chimeric vectors, which should be worth pursuing in the future. Recently Akache *et al.* reported the discovery of cathepsins B/L as possible endosomal uncoating factors.[28] These cysteine proteases are able to bind and cleave AAV2 and AAV8 capsids, with differential cleavage patterns and efficiencies. We are investigating how these cleavages may be related to the subsequent nuclear uncoating process. Ultimately, we hope the availability of these chimeric vectors will not only help us narrow down the functionally relevant capsid regions, but also facilitate the discovery of specific host factors involved in AAV vector transduction.

MATERIALS AND METHODS

Cloning of chimeric AAV capsid packaging helper plasmids. All the AAV packaging helpers used in this study were based on pHLP19-2 (ref. 21), which expresses AAV2 rep and capsid proteins. The coding region for AAV8 capsid was excised from p5E18V2/8 (ref. 4) and used to replace the corresponding region coding for AAV2 capsid in pHLP19-2, thereby generating pHLP-A8, which expresses AAV2 rep and AAV8 capsid proteins. A series of new packaging helpers were constructed on the basis of pHLP19-2 and pHLP-A8 to carry the AAV2 *rep* gene and chimeric *cap* genes. First, *Bsi*WI was used to cut the *cap* genes of both AAV2 and AAV8 in the middle and the N- and C-terminal parts from the two serotypes were swapped to generate chimeric constructs DS1 and DS2. Second, a series of PCR primers were used to amplify the following regions of the AAV2 *cap* gene: a.a. residues 1–209, 210–350, 351–641, and 642–735. Because of the high sequence homology between AAV2 and AAV8 *cap* genes at the sites where those primers were designed, they could be used to amplify the corresponding regions of the AAV8 *cap* gene as well. In combination with *Bsi*WI digestion, a series of *cap* gene fragments were generated for both AAV2 and AAV8, which covered each of the following regions respectively: the N-terminal VP1/2 specific region, interstrand Loop domains I and II, Loop domain III, Loop domain IV, and Loop domain V. The resulting DNA fragments of one serotype were in turn used as megaprimers for a second round of PCR to amplify toward the N- and C-termini on the template containing the *cap* gene of the other serotype, thereby generating products containing chimeric *cap* genes. The PCR products were used to transform *Escherichia coli* after *Dpn*I digestion, which left only PCR products to be repaired and amplified in the bacteria. The final products were cleaved with *Hin*dIII and *Pme*I, and the *cap* gene coding fragments were inserted back into the pHLP19-2 backbone with the corresponding AAV2 *cap* gene fragment removed. This step helped remove any possible mutations introduced by PCR in the *rep* gene or other parts of the helper plasmid. Chimeric constructs DS3–DS18 were generated in this manner. Additionally, more chimeric constructs LIV2.1–2.4, LIV2.14, and LIV8.1–8.4 were made with the same strategy, representing the replacements of individual subloops in the large Loop IV domain of AAV2 and AAV8. A detailed diagram of these chimeric *cap* gene constructs is shown in **Figure 2**. All the chimeric *cap* genes were confirmed by DNA sequencing.

Production of AAV vectors. AAV vectors were produced by a standard calcium–phosphate triple-transfection method.[29] Briefly, 293 cells were transfected with equal amounts of the following plasmids: the AAV packaging helper containing the *rep* and *cap* genes, the adenoviral helper pladeno5, and phFIX-CM1 (ref. 30) containing a liver-specific hFIX transgene expression cassette enclosed between AAV2 inverted terminal repeats . For small-scale AAV packaging analysis, transfections were carried out in 6-cm culture dishes by using ~6×10^5 293 cells per dish and 2 μg of each plasmid. Cells were incubated for 3 days following transfection before harvesting. The crude AAV particle-containing extracts were prepared by subjecting the cells to three consecutive freeze–thaw cycles. Without further AAV purification, these crude extracts were treated with DNase I (Roche, Indianapolis, IN) and Proteinase K (Invitrogen, Carlsbad, CA) subsequently, before the packaged AAV viral genomes were extracted with the Wako DNA extractor kit (Wako Chemicals USA, Richmond, VA) and quantitated by dot blot titration.[21]

For preparative large-scale productions, 25 T225 (Corning, Corning, NY) flasks of 293 cells were transfected for each AAV preparation. The cells were transfected with 25 μg of each plasmid DNA per flask. After 3 days, cells were harvested and subjected to a standard AAV purification procedure including two rounds of cesium chloride gradient ultracentrifugation for purification, ultrafiltration–diafiltration (Amersham, Piscataway, NJ) for cesium chloride removal and particle concentration, and dot blot titration.[21] This procedure has proved to be a reliable method for purification of AAV vectors of different serotypes, regardless of the distinctive binding affinities of their capsids. Final viral preparations

were kept frozen at –80 °C in phosphate-buffered saline containing 5% sorbitol.

Animal procedures. Seven to nine-week-old female C57BL/6 mice were obtained from Jackson Laboratory (Bar Harbor, ME). All animal procedures were conducted according to the animal care guidelines at Stanford University. Portal vein infusion of AAV vectors was carried out as earlier described.[31] Blood samples were collected from the retro-orbital plexus at various points of time following the infusion. After 3 months, the mice were killed and tissue samples were collected from the liver, pancreas, spleen, heart, lung, kidney, intestine, and skeletal muscle (from hind legs).

Enzyme-linked immunosorbent assay and Southern blot analysis. Measurements of hFIX levels in mouse plasma were carried out by an hFIX-specific enzyme-linked immunosorbent assay procedure as reported previously.[32] For Southern blot, total DNA was extracted from the collected tissue samples using a previously reported phenol-free method.[33] To analyze vector DNA copy numbers in different tissues, 20 μg of each DNA sample was digested with *Pst*I in an overnight reaction, separated on 0.8% agarose gels and transferred to positively charged nylon membranes (Amersham, Piscataway, NJ). A series of specific amounts of digested phFIX-CM1 plasmid were used as the standard to calculate the numbers of double-stranded vgs per diploid genome equivalent. All DNAs were detected with radioactively labeled probes, and band intensities were quantitated by phosphorimaging to determine the vector copy number for each sample.

ACKNOWLEDGMENTS

We thank Hui Xu (Stanford University) for her assistance with the animal studies. This work was supported by a grant from the National Institutes of Health (NHLBI 64274).

REFERENCES

1. Chirmule, N, Propert, K, Magosin, S, Qian, Y, Qian, R and Wilson, J (1999). Immune responses to adenovirus and adeno-associated virus in humans. *Gene Ther* **6**: 1574–1583.
2. Erles, K, Sebokova, P and Schlehofer, JR (1999). Update on the prevalence of serum antibodies (IgG and IgM) to adeno-associated virus (AAV). *J Med Virol* **59**: 406–411.
3. Moskalenko, M, Chen, L, van Roey, M, Donahue, BA, Snyder, RO, McArthur, JG *et al.* (2000). Epitope mapping of human anti-adeno-associated virus type 2 neutralizing antibodies: implications for gene therapy and virus structure. *J Virol* **74**: 1761–1766.
4. Gao, GP, Alvira, MR, Wang, L, Calcedo, R, Johnston, J and Wilson, JM (2002). Novel adeno-associated viruses from rhesus monkeys as vectors for human gene therapy. *Proc Natl Acad Sci USA* **99**: 11854–11859.
5. Gao, G, Alvira, MR, Somanathan, S, Lu, Y, Vandenberghe, LH, Rux, JJ *et al.* (2003). Adeno-associated viruses undergo substantial evolution in primates during natural infections. *Proc Natl Acad Sci USA* **100**: 6081–6086.
6. Gao, G, Vandenberghe, LH, Alvira, MR, Lu, Y, Calcedo, R, Zhou, X *et al.* (2004). Clades of adeno-associated viruses are widely disseminated in human tissues. *J Virol* **78**: 6381–6388.
7. Schmidt, M, Grot, E, Cervenka, P, Wainer, S, Buck, C and Chiorini, JA (2006). Identification and characterization of novel adeno-associated virus isolates in ATCC virus stocks. *J Virol* **80**: 5082–5085.
8. Schmidt, M, Katano, H, Bossis, I and Chiorini, JA (2004). Cloning and characterization of a bovine adeno-associated virus. *J Virol* **78**: 6509–6516.
9. Bossis, I and Chiorini, JA (2003). Cloning of an avian adeno-associated virus (AAAV) and generation of recombinant AAAV particles. *J Virol* **77**: 6799–6810.
10. Lochrie, MA, Tatsuno, GP, Arbetman, AE, Jones, K, Pater, C, Smith, PH *et al.* (2006). Adeno-associated virus (AAV) capsid genes isolated from rat and mouse liver genomic DNA define two new AAV species distantly related to AAV-5. *Virology* **353**: 68–82.
11. Nakai, H, Fuess, S, Storm, TA, Muramatsu, S, Nara, Y and Kay, MA (2005). Unrestricted hepatocyte transduction with adeno-associated virus serotype 8 vectors in mice. *J Virol* **79**: 214–224.
12. Wang, Z, Zhu, T, Qiao, C, Zhou, L, Wang, B, Zhang, J *et al.* (2005). Adeno-associated virus serotype 8 efficiently delivers genes to muscle and heart. *Nat Biotechnol* **23**: 321–328.
13. Nakai, H, Thomas, CE, Storm, TA, Fuess, S, Powell, S, Wright, JF *et al.* (2002). A limited number of transducible hepatocytes restricts a wide-range linear vector dose response in recombinant adeno-associated virus-mediated liver transduction. *J Virol* **76**: 11343–11349.
14. Thomas, CE, Storm, TA, Huang, Z and Kay, MA (2004). Rapid uncoating of vector genomes is the key to efficient liver transduction with pseudotyped adeno-associated virus vectors. *J Virol* **78**: 3110–3122.
15. Xie, Q, Bu, W, Bhatia, S, Hare, J, Somasundaram, T, Azzi, A *et al.* (2002). The atomic structure of adeno-associated virus (AAV-2), a vector for human gene therapy. *Proc Natl Acad Sci USA* **99**: 10405–10410.
16. Padron, E, Bowman, V, Kaludov, N, Govindasamy, L, Levy, H, Nick, P *et al.* (2005). Structure of adeno-associated virus type 4. *J Virol* **79**: 5047–5058.
17. Walters, RW, Agbandje-McKenna, M, Bowman, VD, Moninger, TO, Olson, NH, Seiler, M *et al.* (2004). Structure of adeno-associated virus serotype 5. *J Virol* **78**: 3361–3371.
18. Lane, MD, Nam, HJ, Padron, E, Gurda-Whitaker, B, Kohlbrenner, E, Aslanidi, G *et al.* (2005). Production, purification, crystallization and preliminary X-ray analysis of adeno-associated virus serotype 8. *Acta Crystallograph Sect F Struct Biol Cryst Commun* **61**: 558–561.
19. Chapman, MS and Rossmann, MG (1993). Structure, sequence, and function correlations among parvoviruses. *Virology* **194**: 491–508.
20. Hauck, B and Xiao, W (2003). Characterization of tissue tropism determinants of adeno-associated virus type 1. *J Virol* **77**: 2768–2774.
21. Grimm, D, Zhou, S, Nakai, H, Thomas, CE, Storm, TA, Fuess, S *et al.* (2003). Preclinical *in vivo* evaluation of pseudotyped adeno-associated virus vectors for liver gene therapy. *Blood* **102**: 2412–2419.
22. Nakai, H, Iwaki, Y, Kay, MA and Couto, LB (1999). Isolation of recombinant adeno-associated virus vector-cellular DNA junctions from mouse liver. *J Virol* **73**: 5438–5447.
23. Sarkar, R, Tetreault, R, Gao, G, Wang, L, Bell, P, Chandler, R *et al.* (2004). Total correction of hemophilia A mice with canine FVIII using an AAV 8 serotype. *Blood* **103**: 1253–1260.
24. Grimm, D, Pandey, K, Nakai, H, Storm, TA and Kay, MA (2006). Liver transduction with recombinant adeno-associated virus is primarily restricted by capsid serotype not vector genotype. *J Virol* **80**: 426–439.
25. Opie, SR, Warrington, KH Jr., Agbandje-McKenna, M, Zolotukhin, S and Muzyczka, N (2003). Identification of amino acid residues in the capsid proteins of adeno-associated virus type 2 that contribute to heparan sulfate proteoglycan binding. *J Virol* **77**: 6995–7006.
26. Perabo, L, Goldnau, D, White, K, Endell, J, Boucas, J, Humme, S *et al.* (2006). Heparan sulfate proteoglycan binding properties of adeno-associated virus retargeting mutants and consequences for their *in vivo* tropism. *J Virol* **80**: 7265–7269.
27. Akache, B, Grimm, D, Pandey, K, Yant, SR, Xu, H and Kay, MA (2006). The 37/67-kilodalton laminin receptor is a receptor for adeno-associated virus serotypes 8, 2, 3, and 9. *J Virol* **80**: 9831–9836.
28. Akache, B, Grimm, D, Shen, X, Fuess, S, Yant, SR, Glazer, DS *et al.* (2007). A two-hybrid screen identifies cathepsins B and L as uncoating factors for adeno-associated virus 2 and 8. *Mol Ther* **15**: 330–339.
29. Grimm, D (2002). Production methods for gene transfer vectors based on adeno-associated virus serotypes. *Methods* **28**: 146–157.
30. Miao, CH, Nakai, H, Thompson, AR, Storm, TA, Chiu, W, Snyder, RO *et al.* (2000). Nonrandom transduction of recombinant adeno-associated virus vectors in mouse hepatocytes *in vivo*: cell cycling does not influence hepatocyte transduction. *J Virol* **74**: 3793–3803.
31. Nakai, H, Herzog, RW, Hagstrom, JN, Walter, J, Kung, SH, Yang, EY *et al.* (1998). Adeno-associated viral vector-mediated gene transfer of human blood coagulation factor IX into mouse liver. *Blood* **91**: 4600–4607.
32. Nakai, H, Yant, SR, Storm, TA, Fuess, S, Meuse, L and Kay, MA (2001). Extrachromosomal recombinant adeno-associated virus vector genomes are primarily responsible for stable liver transduction *in vivo*. *J Virol* **75**: 6969–6976.
33. Chen, ZY, Yant, SR, He, CY, Meuse, L, Shen, S and Kay, MA (2001). Linear DNAs concatemerize *in vivo* and result in sustained transgene expression in mouse liver. *Mol Ther* **3**: 403–410.
34. Guex, N and Peitsch, MC (1997). SWISS-MODEL and the Swiss-PdbViewer: an environment for comparative protein modeling. *Electrophoresis* **18**: 2714–2723.